Geochimica et Cosmochimica Acta, Vol. 68, No. 24, pp. 5189–5195, 2004

0016-7037/04 $30.00 + .00

doi:10.1016/j.gca.2004.07.015

Determination of the second critical end point in silicate-H_2O systems using high-pressure and high-temperature X-ray radiography

KENJI MIBE,[1,2,*] MASAMI KANZAKI,[3] TATSUHIKO KAWAMOTO,[4] KYOKO N. MATSUKAGE,[5] YINGWEI FEI,[1] and SHIGEAKI ONO[6]

[1]Geophysical Laboratory, Carnegie Institution of Washington, 5251 Broad Branch Road, Washington, DC 20015-1305, USA
[2]Earthquake Research Institute, University of Tokyo, 1-1-1 Yayoi, Bunkyo-ku, Tokyo 113-0032, Japan
[3]Institute for Study of the Earth's Interior, Okayama University, Misasa, Tottori 682-0193, Japan
[4]Institute for Geothermal Sciences, Graduate School of Science, Kyoto University, Beppu 874-0903, Japan
[5]Department of Environmental Science, Ibaraki University, 2-1-1 Bunkyo, Mito, Ibaraki 310-0056, Japan
[6]Institute for Research on Earth Evolution, Japan Agency for Marine-Earth Science and Technology, 2-15 Natsushima-cho, Yokosuka, Kanagawa 237-0061, Japan

(*Received January* 23, 2004; *accepted in revised form July* 20, 2004)

Abstract—To determine the second critical end point in silicate-H_2O systems, a new method for the direct observations of immiscible fluids has been developed using a synchrotron X-ray radiography technique. High-pressure and high-temperature experiments were carried out with a Kawai-type, double-stage, multi-anvil high-pressure apparatus (SPEED-1500) installed at BL04B1, SPring-8, Japan. The Sr-plagioclase ($SrAl_2Si_2O_8$)-H_2O system was used as an illustrative example. A new sample container composed of a metal (Pt) tube with a pair of lids, made of single crystal diamonds, was used under pressures between 3.0 and 4.3 GPa, and temperatures up to ~1600°C. The sample in the container could be directly observed through the diamond lids with X-ray radiography. At around 980 to 1060°C and pressures between 3.0 and 4.0 GPa, light gray spherical bubbles moving upward through the dark gray matrix were observed. The light gray spheres that absorb less X-rays represent an aqueous fluid, whereas the dark gray matrix represents a silicate melt. These two immiscible phases (aqueous fluid and silicate melt) were observed up to 4.0 GPa. At 4.3 GPa, no bubbles were observed. These observations suggest that the second critical end point in the Sr-plagioclase-H_2O system occurs at around 4.2 ± 0.2 GPa and 1020 ± 50°C. Our new technique can be applied to the direct observations of various systems with two coexisting fluids under deep mantle conditions.

1. INTRODUCTION

H_2O is the dominant volatile component in the Earth's interior. It affects the melting temperature of rocks (e.g., Yoder et al., 1957), the composition of magmas generated (e.g., Kushiro, 1972), and the rheology of rocks (e.g., Karato et al., 1986). Therefore, understanding the phase relations in silicate-H_2O systems is fundamental for clarifying the physical and chemical evolution of the Earth. At the conditions corresponding to the Earth's crust and upper mantle, two types of mobile phases (aqueous fluid and hydrous silicate melt) can coexist in silicate-H_2O systems. In general, both the solubility of water in silicate melt (e.g., Hodges, 1974) and the solubility of silicate materials in aqueous fluid (e.g., Nakamura and Kushiro, 1974) increase with increasing pressure. At the second critical end point, silicate melt and aqueous fluid in the Earth's interior are expected to become indistinguishable from each other (e.g., Niggli, 1920; Wyllie and Tuttle, 1960).

Kennedy et al. (1962) determined the second critical end point in the SiO_2-H_2O system by measuring the composition of aqueous fluid and melt quenched from high pressure and high temperature. They reported that the second critical end point in the SiO_2-H_2O system should occur at 0.97 GPa and 1080°C. In the system albite-H_2O, Paillat et al. (1992) concluded that the second critical end point should occur at around 1.5 GPa and 670°C by an analysis of all the available data on water solubility in albite melt. In other silicate-H_2O systems which are more relevant to the Earth's crust and upper mantle, the second critical end point has not yet been determined. This is because phase identification of the quenched samples obtained by high-pressure and high-temperature experiments can be very difficult (e.g., Mibe et al., 2002).

Shen and Keppler (1997) succeeded in the direct observation of complete miscibility between aqueous fluid and silicate melt using a hydrothermal diamond anvil cell (Bassett et al., 1993). Using this hydrothermal diamond anvil cell technique, the critical curves have been determined in various silicate-H_2O systems with a wide range of melt compositions, including albite (Shen and Keppler, 1997), albite with excess Na_2O, B_2O_3, and F_2O_{-1} (Sowerby and Keppler, 2002), nepheline, jadeite, dacite, haplogranite, Ca-bearing granite (Bureau and Keppler, 1999), and natural andesite and rhyolite (Kawamoto, 2004).

Once the critical curve has been determined, the second critical end point can be obtained by the intersection between the critical curve and the H_2O-saturated solidus. However, in the systems with a high solidus temperature such as basalt-H_2O (Bureau and Keppler, 1999, Kawamoto, 2004) and peridotite-H_2O, the limitation on the hydrothermal diamond anvil cell prevent one from attaining a high enough temperature to observe the aqueous fluid and silicate melt. We developed, therefore, a new method for the direct observation of 2-fluids coexisting at high-pressure and high-temperature conditions. Here we report our new technique, and its application to the deter-

* Author to whom correspondence should be addressed (mibe@eri.u-tokyo.ac.jp).

mination of the second critical end point in Sr-plagioclase ($SrAl_2Si_2O_8$)-H_2O system.

2. EXPERIMENTAL METHOD

2.1. Experimental Procedure

Experiments were carried out using an X-ray radiography technique (Kanzaki et al., 1987) together with Kawai-type, double-stage, multi-anvil system driven by DIA-type cubic press (SPEED-1500) installed at BL04B1 (Utsumi et al., 1998), SPring-8, Japan. A direct white X-ray beam, which passes through the anvil gaps of SPEED-1500 and the sample under high pressure, was observed with an X-ray camera (Fig. 1). Real time radiographic images were recorded with a digital video camera or a hard disk video recorder. The spatial resolution of the sample image was ~5 μm. The exposure time for the X-ray camera was ~35 ms. The capability of the system in BL04B1, SPring-8 is described in Funakoshi et al. (2000). Tungsten carbide (WC) cubes, having 11 mm corner truncation edges, were used as the second-stage anvils. A semisintered chromium-doped MgO octahedron (18-mm octahedron edge length) was used as the pressure medium. Twelve pieces of preformed pyrophyllite gaskets were used, and graphite is used as an X-ray "window" material through two of the gaskets, put on the upstream and downstream side of the X-ray path. A semisintered ZrO_2 sleeve was used as a thermal insulator, and a cylindrical graphite heater was inserted parallel to the X-ray. A pair of Mo foils with a hole (2.7 mm diameter) were used as electrodes.

The Strontium-plagioclase, ($SrAl_2Si_2O_8$)-H_2O, system was used as a starting material to obtain enough contrast in the radiographic images. Sr-bearing silicate melt has a higher average atomic weight, thus would absorb X-rays more efficiently compared to the aqueous fluid phase. Reagent grade $Sr(OH)_2 \cdot 8H_2O$, Al_2O_3, and SiO_2 were mixed in an appropriate ratio. In addition to the water included as hydroxide, deionized water was added to the sample powder by a micro syringe.

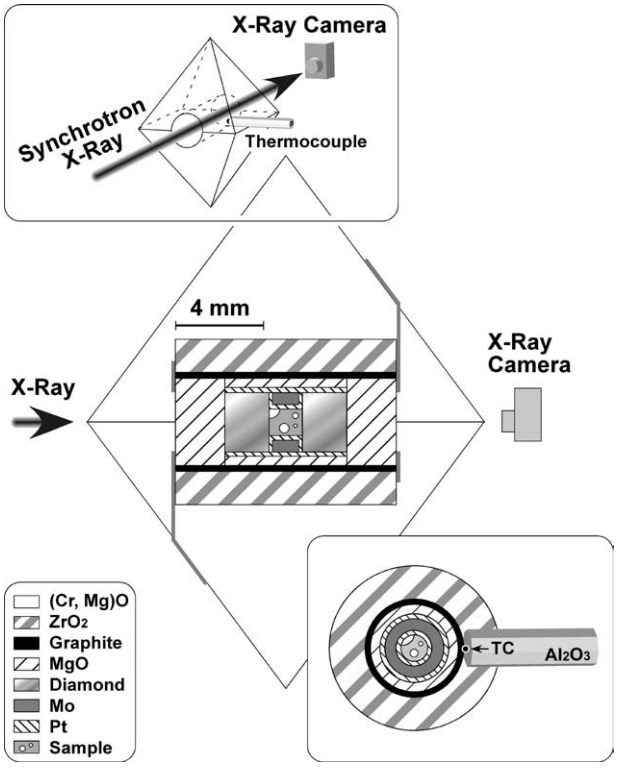

Fig. 1. Experimental configuration and furnace assembly used in high pressure and temperature experiments. The X-ray camera is not to scale. The position of the hot junction of thermocouple is illustrated in the lower right hand frame.

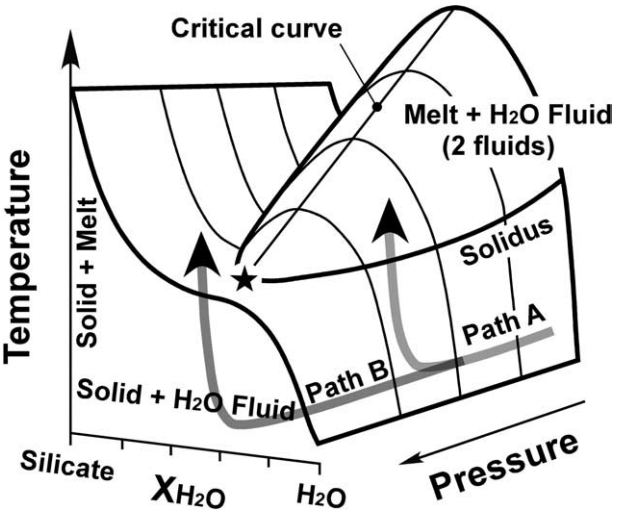

Fig. 2. Pressure-temperature paths during experiments (modified after Stalder et al., 2001). At conditions below the second critical end point (star) the equilibrium assemblage, melt (hydrous silicate magma) + H_2O Fluid (aqueous fluid), can be obtained during heating under pressure (Path A). Beyond the second critical end point, only one fluid phase (i.e., supercritical fluid) exists during heating (Path B).

The total amount of H_2O in the starting materials was 45 ± 5 and 55 ± 5 wt%.

The sample container should not react with hydrous samples, but needs to be X-ray transparent. Therefore, we developed a new sample container, which is composed of a platinum tube and a pair of single crystal diamond lids (2.7 mm diameter; 2.0 mm height) placed on both ends of the platinum tube (Fig. 1). The sample, contained inside the tube, can be directly observed through the diamond lids and an aperture in the platinum tube. The central platinum tube and two diamond lids are surrounded by a larger platinum tube. This outer tube helps to seal water when the sample is pressurized at room temperature.

In the experiments at pressures below the second critical end point, the experimental P-T path intersects the stability field of aqueous fluid + silicate melt (Path A in Fig. 2). In this case, one phase (either aqueous fluid or silicate melt) would be assumed to be a spherical shape in the other phase because of the differences in their interfacial tension. Therefore, a round shape is expected to be observed in the radiographic images. On the other hand, in experiments beyond the second critical end point, such evidence of two coexisting fluids should not be observed, because a supercritical fluid is the only phase that exists at these high-temperature conditions (Path B in Fig. 2).

The radiographic experiments were performed at pressures of 3.0 to 4.3 GPa, and temperatures ranging up to ~1600°C. After observing with the X-ray camera, the samples were quenched from the desired P-T conditions so that the X-ray radiographic images could be compared with the quenched textures. The X-ray camera was on continuously through duration of the experiment, and images were recorded from the beginning of heating until quench.

2.2. Pressure-Temperature Calibrations

The temperature of the sample was monitored with a W5%Re-W26%Re thermocouple. The high-temperature junction of the thermocouple was guided by an aluminum electrical insulator through a small hole in ZrO_2 sleeve, and placed in contact with the surface of the graphite heater (Fig. 1). No correction for the effect of pressure on the thermocouple emf was applied. Pressure calibrations were done at room temperature and 800°C by a separate series of experiments (Table 1) using an identical cell assembly as in the radiographic experiments. X-ray diffraction patterns were collected from a 100 × 200 μm area of the pressure marker (a mixture of finely powdered, reagent grade Au and NaCl) using an energy-dispersive, pure-Ge, semiconducting, solid-

Table 1. Experimental conditions and results for pressure-temperature calibration.[a]

Run	Load (ton)	T (°C)	$(V/V_0)_{Au}$	$(V/V_0)_{NaCl}$	P_{Au} (GPa)	P_{NaCl} (GPa)
s1020	120	25	0.9972 (5)	0.9773 (5)	0.45 (8)	0.58 (1)
	200	25	0.9904 (4)	0.9388 (17)	1.64 (8)	1.75 (6)
	300	25	0.9821 (3)	0.9030 (8)	3.15 (6)	3.11 (4)
	350	25	0.9768 (8)	0.8880 (12)	4.15 (16)	3.77 (5)
	350	800	1.0174 (2)	0.9578 (6)	2.93 (3)	3.39 (2)
	350	850	1.0174 (2)	0.9578 (6)	3.30 (3)	3.54 (2)
	350	900	1.0174 (2)	0.9578 (6)	3.67 (3)	3.68 (2)
	350	950	1.0174 (2)	0.9578 (6)	4.03 (3)	3.83 (2)
s1057	120	25	0.9977 (5)	0.9816 (5)	0.37 (8)	0.46 (1)
	150	25	0.9950 (4)	0.9656 (2)	0.83 (7)	0.91 (1)
	180	25	0.9923 (5)	0.9525 (2)	1.31 (8)	1.30 (1)
	200	25	0.9905 (6)	0.9433 (3)	1.63 (11)	1.60 (1)
	200	800	1.0322 (2)	1.0429 (41)	0.96 (3)	1.35 (8)
	200	850	1.0322 (2)	1.0429 (41)	1.33 (3)	1.50 (8)
	200	900	1.0322 (2)	1.0429 (41)	1.71 (3)	1.64 (8)
	200	950	1.0322 (2)	1.0429 (41)	2.09 (3)	1.79 (8)
s1058	120	25	0.9984 (2)	0.9837 (3)	0.26 (3)	0.41 (1)
	150	25	0.9957 (5)	0.9681 (4)	0.72 (9)	0.83 (1)
	180	25	0.9925 (5)	0.9544 (5)	1.27 (8)	1.24 (2)
	200	25	0.9916 (2)	0.9472 (5)	1.43 (4)	1.47 (2)
	250	25	0.9878 (5)	0.9295 (7)	2.11 (9)	2.08 (3)
	280	25	0.9857 (4)	0.9202 (8)	2.48 (7)	2.42 (3)
	300	25	0.9850 (5)	0.9160 (7)	2.62 (9)	2.58 (3)
	350	25	0.9810 (3)	0.9028 (7)	3.35 (6)	3.12 (3)
	400	25	0.9785 (3)	0.8912 (4)	3.83 (5)	3.62 (2)
s1059	400	25	0.9747 (5)	0.8797 (5)	4.56 (10)	4.16 (2)
	400	800	1.0162 (3)	0.9519 (12)	3.10 (4)	3.57 (4)
	400	850	1.0162 (3)	0.9519 (12)	3.46 (4)	3.72 (4)
	400	900	1.0162 (3)	0.9519 (12)	3.83 (4)	3.87 (4)
	400	950	1.0162 (3)	0.9519 (12)	4.20 (4)	4.01 (4)
s1060	300	25	0.9829 (4)	0.9123 (5)	3.00 (7)	2.73 (2)
s1072	500	25	0.9718 (4)	0.8698 (4)	5.15 (7)	4.66 (2)
	500	800	1.0113 (4)	0.9324 (4)	3.81 (5)	4.23 (1)
	500	850	1.0113 (4)	0.9324 (4)	4.17 (5)	4.37 (1)
	500	900	1.0113 (4)	0.9324 (4)	4.54 (5)	4.52 (1)
	500	950	1.0113 (4)	0.9324 (4)	4.90 (5)	4.67 (1)

[a] Numbers in parentheses represent the last digits of the standard deviations.
High-temperature calibrations were done at thermocouple temperature (T_{TC}) of 800°C.

state detector set at a fixed diffraction angle, 2θ, of ~5°. The diffraction angle was calibrated based on the unit cell volume of Au and NaCl measured at room pressure and temperature. The unit cell volumes were calculated from diffraction peaks, and then pressure was determined by the P-V-T equation of state of Au proposed by Anderson et al. (1989) and of NaCl by Decker (1971).

In the pressure calculation at high-temperature conditions, the corrected temperature (referred as "realistic sample temperature = T_R," hereafter) was used instead of the thermocouple temperature (T_{TC}), because the high-temperature junction of the thermocouple was too far away from the sample chamber (Fig. 1). The configuration of the cell assembly used in the present study makes it difficult to correct the temperature based on simultaneous, direct measurements of T_{TC} and T_R using two pairs of thermocouples. T_R was, therefore, estimated using Au and NaCl pressure scales, following the method of Yagi et al. (1985).

The differences in the pressures obtained from Au (P_{Au}) and NaCl (P_{NaCl}) using various temperature values are plotted in Figure 3. Note that all these high-temperature calibrations were done at T_{TC} = 800°C. However, all the curves in Figure 3 have the minima in the vicinity of 900°C, regardless of the experimental load. Therefore, based on the assumption that P_{Au} and P_{NaCl} should be the same at high temperature, we have concluded that the realistic sample temperature (T_R) at T_{TC} = 800°C should be 900°C. Then, by fitting the points (T_R, T_{TC}) = (25, 25) and (900, 800), a linear correlation between T_R and T_{TC} can be obtained as follows;

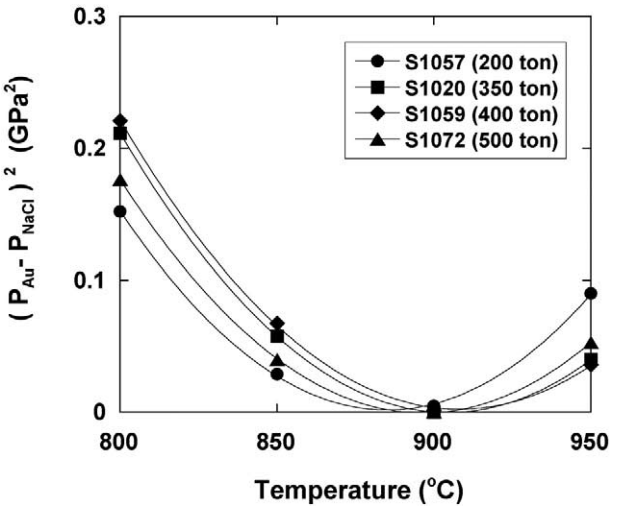

Fig. 3. The squared difference of P_{AU} and P_{NaCl} against temperature. Actual high-temperature calibrations were conducted at T_{TC} = 800°C. Note that all curves have the minima at around 900°C regardless of the experimental load. Data are from Table 1.

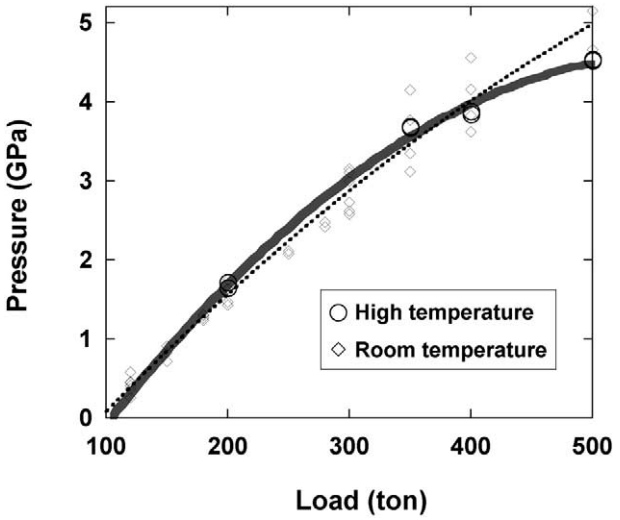

Fig. 4. Pressure-load calibration curves for SPEED-1500 at SPring-8. Shaded and dotted curves represent the second-order polynomial fit of high-temperature (T_{TC} = 800°C) data (including P_{Au} and P_{NaCl}) and room-temperature data (also including P_{Au} and P_{NaCl}), respectively. Data are from Table 1.

$$T_R(°C) = 1.129 \times T_{TC}(°C) - 3.326 \quad (1)$$

Here, we used the linear fitting because we had only two data points to fit. As we extrapolate further away from these known values, an estimate of T_R becomes unreliable fairly quickly. Clearly, a more detailed temperature calibration is needed for higher temperature experiments in future work.

The relationship between experimental load and sample pressure, using T_R, is shown in Figure 4. This pressure-load relation is used to estimate the experimental pressure in the radiographic experiments. The difference of the pressures measured at both high temperature and room temperature is very small, until the load reaches above 450 to 500 tons, at which point there is a slight decrease (0.3 ~ 0.5 GPa) in pressure with heating (Table 1 and Fig. 4). The error in the temperature (T_R) determination is about ± 50°C and that of the pressure is about ± 0.2 GPa. In the following sections, all the temperatures that are shown are T_R values.

2.3. Examination of the Recovered Samples

First, the diamonds were removed from the recovered samples and inspected. Small etch pits were seen on the surface that was in contact with the hydrous sample during the run. This indicates that some amount of carbon might have been dissolved in the sample under experimental conditions. These etch pits are prominent in samples that were heated and kept for a long time above 1400°C. In the experiments below 1400°C, however, etch pits are tiny and carbon contamination in the system should be negligible. Usually, the single crystal diamonds can be used for multiple experimental runs, as long as they are not cracked.

Both surfaces of the samples which were in contact with diamonds, were inspected with a microscope. After the surface inspection, the samples were ground and polished step by step in order not to overlook any voids. They were observed with a microscope between grinding periods to check for possible voids. Some samples that were quenched from lower temperatures contain a crystalline phase which was considered to be an equilibrium phase at the quenched conditions. Quantitative analyses using JEOL 8900 electron microprobe at Geophysical Laboratory showed that these crystals were corundum.

3. RESULTS

The experimental conditions and the results are summarized in Table 2. At around 980 to 1060°C and up to 4.0 GPa, some light gray, spherical bubbles (50–500 μm in diameter) were observed to be moving upward through the dark gray matrix. The light gray spherules absorbed less X-rays, and are considered to be the aqueous fluid phase, whereas the dark gray matrix is a silicate melt. When temperature was increased further, small bubbles coalesced to form a larger bubble. Subsequently, the larger bubbles became hemispheres wetting the upper wall of the metal tube (Fig. 5).

The temperature range, in which both aqueous fluid and silicate melt were observed, is shown in Table 2. When fluid bubbles are moving upward in the silicate matrix, it is easy to identify the phases. With increasing temperature, however, phase identification in radiographic images becomes more difficult. This is because the aqueous fluid and the silicate melt separate much more quickly, due to the viscosity reduction of both phases. After separating, the aqueous fluid in Sr-plagioclase-H_2O system tends to wet the diamonds and covers both sides of the silicate melt (Figs. 6A,B). Once the aqueous fluid and silicate melt had a geometrical arrangement such as shown in Figures 6A,B, the contrast in the radiographic images became weaker. This usually happened when the temperature approached 1600°C. Furthermore, the platinum tube used as a sample container becomes softer and deforms at temperature slightly higher than 1600°C. Further increase in temperature

Table 2. Experimental conditions and results.

Run	P (GPa)	T_{MAX}[a] (°C)	T_{Quench}[b] (°C)	H_2O[c] (wt%)	Observed phases in X-ray images	Quench Products
S907	3.0	1600 (1420)	640 (570)	45	Fluid + melt (990–1440°C)[d]	n.d.[e]
DW-1[f]	3.0	1460 (1300)	1460 (1300)	45	—	Glass + void + Al_2O_3
S914	3.0	1600 (1420)	1520 (1350)	45	Fluid + melt (1050–1590°C)	Glass + void
S1074	3.6	1610 (1430)	1610 (1430)	55	Fluid + melt (1060–1580°C)	Glass + void
S1071	4.0	1610 (1430)	1520 (1350)	55	Fluid + melt (980–1610°C)	Glass + void + Al_2O_3
S1075	4.3	1580 (1400)	1260 (1120)	55	Supercritical	Quench crystals
S1073	4.3	1600 (1420)	1460 (1300)	55	Supercritical	Quench crystals

[a] The maximum temperature in T_R value during the run. Numbers in parentheses represent thermocouple temperatures (T_{TC}).
[b] Quenched temperature in T_R value. Numbers in parentheses represent thermocouple temperatures (T_{TC}).
[c] Amount of H_2O in starting materials.
[d] Two phases were observed during temperature (T_R) range shown in parentheses.
[e] Not determined.
[f] Quench experiment was done using 1500-ton Walker-type multianvil press at Geophysical Laboratory.

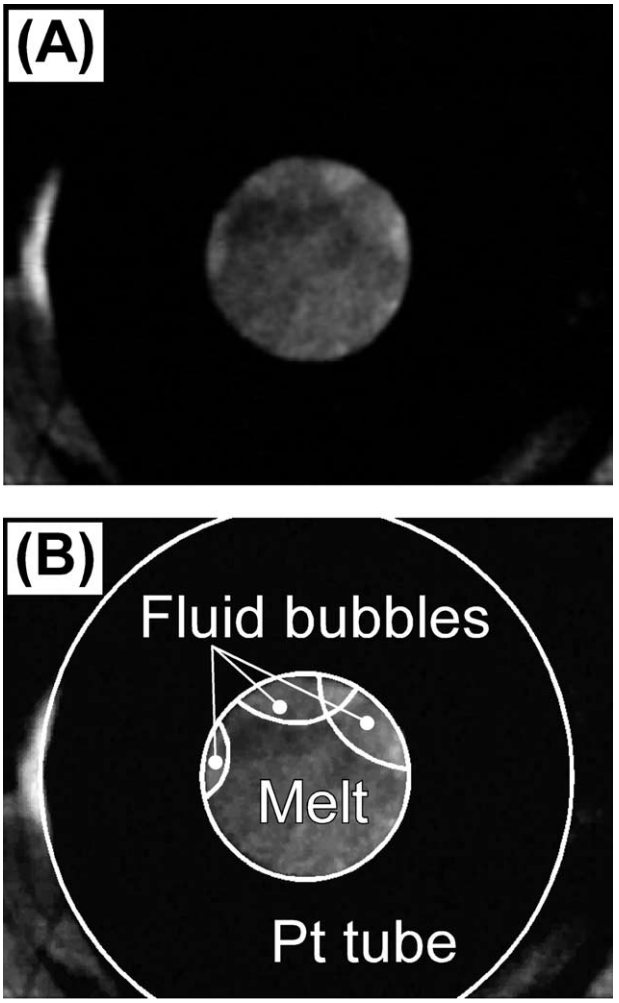

Fig. 5. X-ray radiographic images taken at 3.0 GPa and 1300°C (S914). (A) Image. (B) Explanatory notes along with (A).

always results in loss of radiographic images because of breaking diamond(s). We, therefore, decided not to heat the samples higher than 1600°C, and the upper limits of the temperature range shown in Table 2 do not directly represent the stability limits of the miscibility gap between aqueous fluid and silicate melt.

At least up to 1600°C, two immiscible phases (aqueous fluid and silicate melt) were observed in the experiments up to 4.0 GPa (Table 2). At 4.3 GPa, on the other hand, bubbles were not seen during heating up to ~1600°C.

A photograph of the recovered sample quenched from 3.0 GPa and 1460°C is shown in Figure 6C. A large and hemispherical void, which is considered to be an aqueous fluid phase during the run, can be seen in the glass matrix. The glass matrix, on the other hand, is considered to be silicate melt during the run. This image (Fig. 6C) is consistent with the X-ray radiographic image (Fig. 5) where coalescent light gray bubbles appear in a dark gray matrix at the temperatures between 1050°C and 1590°C in the run number S914 (Table 2). No voids were found in the recovered samples quenched from 4.3 GPa and 1260°C (S1075) and 1460°C (S1073). Instead, quench crystals were homogeneously distributed throughout the entire sample capsules (Fig. 6D).

4. DISCUSSION

Although the temperature gradient in the furnace assembly used in the present study has not been investigated, the multi-anvil press is known to have a larger temperature gradient than the hydrothermal diamond anvil cell. In fluid bearing systems, the high entropy fluid phase (including the liquid) tends to migrate to the hot region in the sample capsule, resulting in chemical differentiation within the experimental charges. This problem makes it difficult to determine the equilibrium phase assemblages at experimental P-T conditions in fluid bearing systems. As described in the previous section and shown in Figure 6C, aqueous fluid moved upward through the silicate melt during heating because it is the lower density phase. With a further increase in temperature, the aqueous fluid coalesced to form larger bubbles and wetted the diamond surfaces (Figs. 6A,B). The initial upward movement of the aqueous fluid can be interpreted as gravitational segregation, and the latter one could be caused by the surface energy relationships among the aqueous fluid, silicate melt, metal tube, and diamond windows. In the present study, therefore, the spatial distribution of aqueous fluid and silicate melt within a sample charge does not seem to be governed by the temperature gradient in the furnace assembly and the temperature gradient does not need to be considered when determining the 2-fluid stability field. It seems reasonable to suppose that both aqueous fluid and silicate melt are stable if the two phases are observable in the radiographic images.

Because the two phases (aqueous fluid and silicate melt) became observable at temperatures between 980 and 1060°C in the experiments at pressures between 3.0 and 4.0 GPa (Table 2), the hydrous solidus in the Sr-plagioclase-H_2O system could be located close to these temperatures at pressures between 3.0 and 4.0 GPa. Considering the large temperature uncertainties, it is concluded that the solidus temperature at 3.0 to 4.0 GPa is 1020 ± 50°C, and appears to be almost constant in this pressure range.

Both radiographic observations and optical inspection of the quenched samples indicate that aqueous fluid and silicate melt can coexist up to 4.0 GPa. Above 4.3 GPa, however, these two phases can no longer be distinguished. Therefore, it can be concluded that the second critical end point in Sr-plagioclase-H_2O system occurs at pressure between 4 and 4.3 GPa. As the second critical end point occurs on the solidus, the temperature of the second critical end point should be close to 1020 ± 50°C.

Shen and Keppler (1997) reported that the water content of a supercritical fluid on the critical curve near the second critical end point in the albite-H_2O system was ~55 wt%. Our starting material for higher pressure experiments in Sr-plagioclase-H_2O system had exactly the same water content. In our experiments, however, it is not easy to determine the water content of the fluid on the second critical end point in Sr-plagioclase-H_2O system. To determine this value precisely, another series of runs, with varying water contents in the starting materials, are required at P-T conditions near the second critical end point. In a strict sense it cannot be ruled out that a small miscibility gap still exists even at 4.3 GPa on

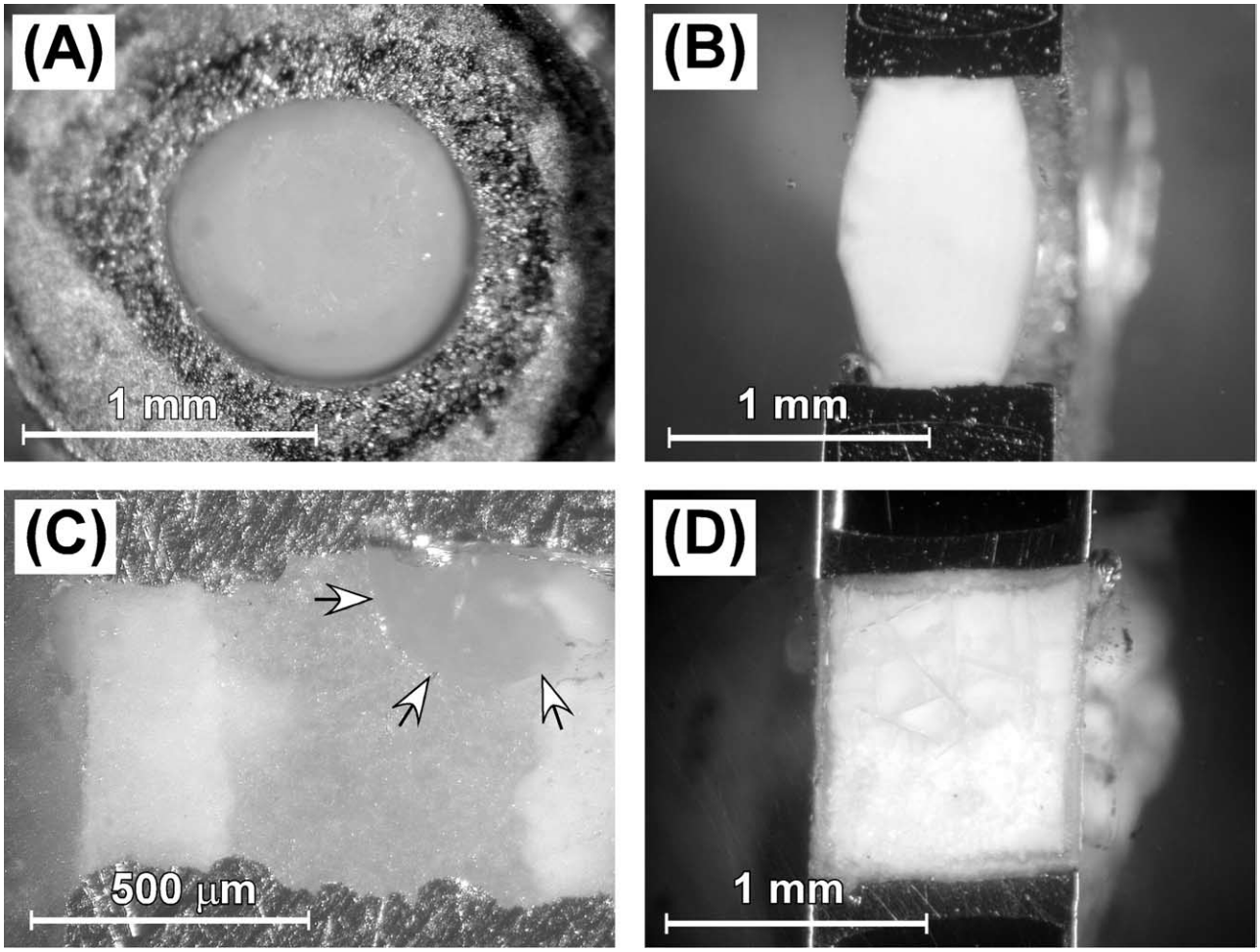

Fig. 6. Images of the recovered samples quenched at (A) 4.0 GPa and 1520°C (S1071), (B) 3.6 GPa and 1610°C (S1074), (C) 3.0 GPa and 1460°C (DW-1), and (D) 4.3 GPa and 1260°C (S1075). (A) is the sample surface, which is faced to the single crystal diamond. This is the same view as the radiographic images shown in Figure 5. (B), (C), and (D) are the polished surfaces, which are parallel to the X-ray path. In (A) and (B), void spaces can be seen on the surfaces faced to the diamond lids. (C) A large hemispherical void space is indicated by white arrows. (D) There is no void space.

either side of 55 wt% H_2O, but the miscibility gap near the second critical end point generally shrinks quickly with a small increase in pressure. Therefore, the second critical end point in Sr-plagioclase-H_2O system is probably close to 4.2 ± 0.2 GPa and 1020 ± 50°C.

Using our new technique, one can directly observe many systems where two fluids coexist at high-pressure and high-temperature conditions that could not be achieved by previous methods (i.e., hydrothermal diamond anvil cell). Since we observe samples "directly," through layers of ceramics using an X-ray camera, with our technique there is a limitation on our ability to identify phases whose composition and density are close to each other. This difficulty is easily understood if we compare the quality of images shown in Figure 5 with those in the studies using the hydrothermal diamond anvil cell (Shen and Keppler, 1997; Bureau and Keppler, 1999; Sowerby and Keppler, 2002; Kawamoto, 2004). Preliminary experiments, however, revealed that the new technique reported here can be also applied to the basalt-H_2O system (Mibe et al., 2003). Detailed studies determining the second critical end point in various silicate-H_2O systems with a wide rage of melt compositions are still needed to achieve a better understanding of the properties of fluids and melts in the Earth's deep interior.

Acknowledgments—We thank K. Funakoshi, T. Fujii, A. Yasuda, S. Urakawa, Y. Nishihara, E. Takahashi, T. Okada, A. Nozawa, Y. Yoshimura, G. H. Gudfinnsson, M. Frank, H. Watson, S. Keshav, and C. Hadidiacos for their helpful comments, discussions, and support in experiments and analyses. Reviews by H. Keppler and two anonymous referees improved the manuscript. This study was partly supported by the Research Fellowships of the Japan Society for the Promotion of Science for Young Scientists, joint research program at Institute for Study of the Earth's Interior, and the Nissan Science Foundation. The synchrotron radiation experiments were performed at the BL04B1 in the SPring-8 with the approval of the Japan Synchrotron Radiation Research Institute (JASRI) (Proposal No. 2002A0333-ND2-np, 2002B0704-CD2-np, 2003A0591-ND2-np, and 2003B0128-ND2b-np).

Associate editor: J. K. Russell

REFERENCES

Anderson O. L., Isaak D. G., and Yamamoto S. (1989) Anharmonicity and the equation of state for gold. *J. Appl. Phys.* **65,** 1534–1543.

Bassett W. A., Shen A. H., Buckum A., and Chou I.-M. (1993) A new diamond anvil cell for hydrothermal studies to 2.5 GPa and from −190°C to 1200°C. *Rev. Sci. Instrum.* **64,** 2340–2345.

Bureau H. and Keppler H. (1999) Complete miscibility between silicate melts and hydrous fluids in the upper mantle: Experimental evidence and geochemical implications. *Earth Planet. Sci. Lett.* **165,** 187–196.

Decker D. L. (1971) High-pressure equation of state for NaCl, KCl and CsCl. *J. Appl. Phys.* **42,** 3239–3244.

Funakoshi K. Kanzaki M., Yasuda A., Suzuki A., Terasaki H., and Yamashita S. (2000) Viscosity measurement of albite melt under high pressure using an in situ X-ray radiography technique. In *Science and Technology of High Pressure: Proceedings of AIRAPT-17* (eds. M. H. Manghnani, W. J. Nellis, and M. F. Nicol), pp. 1023–1026. Universities Press.

Hodges F. N. (1974) The solubility of H_2O in silicate melts. *Year Book Carnegie Inst. Wash.* **73,** 251–255.

Kanzaki M., Kurita K., Fujii T., Kato T., Shimomura O., and Akimoto S. (1987) A new technique to measure the viscosity and density of silicate melts at high pressure. In *High-Pressure Research in Mineral Physics* (eds. M. H. Manghnani and Y. Syono), pp. 195–200. Washington, DC: Am. Geophys. Union.

Karato S., Paterson M. S., and Fitzgerald J. D. (1986) Rheology of synthetic olivine aggregates; influence of grain size and water. *J. Geophys. Res.* **91,** 8151–8176.

Kawamoto T. (2004) Critical phenomena between magmas and aqueous fluid (in Japanese with English abstract). *Rev. High Press. Sci. Tech.* **14,** 235–241.

Kennedy G. C., Wasserburg G. J., Heard H. C., and Newton R. C. (1962) The upper three phase region in the system SiO_2-H_2O. *Am. J. Sci.* **260,** 501–521.

Kushiro I. (1972) Effect of water on the composition of magmas formed at high pressures. *J. Petrol.* **13,** 311–334.

Mibe K., Fujii T., and Yasuda A. (2002) Composition of aqueous fluid coexisting with mantle minerals at high pressure and its bearing on the differentiation of the Earth's mantle. *Geochim. Cosmochim. Acta* **66,** 2273–2285.

Mibe K., Kanzaki M., Kawamoto T., Matsukage K., Fei Y., and Ono S. (2003) Direct observation of immiscible fluids using X-ray radiography (abstract). *Geochim. Cosmochim. Acta* **67** (Suppl. 1), A289.

Nakamura Y. and Kushiro I. (1974) Composition of the gas phase in Mg_2SiO_4-SiO_2-H_2O at 15 kbar. *Year Book Carnegie Inst. Wash.* **73,** 255–258.

Niggli P. (1920) *Die leichtflüchtigen Bestandteile im Magma.* Leipzig: B. G. Teubner.

Paillat O., Elphick S. C., and Brown W. L. (1992) The solubility of water in $NaAlSi_3O_8$ melts: A re-examination of Ab-H_2O phase relationships and critical behaviour at high pressures. *Contrib. Mineral. Petrol.* **112,** 490–500.

Shen A. and Keppler H. (1997) Direct observation of complete miscibility in the albite-H_2O system. *Nature* **385,** 710–712.

Sowerby J. R. and Keppler H. (2002) The effect of fluorine, boron and exess sodium on the critical curve in the albite-H_2O system. *Contrib. Mineral. Petrol.* **143,** 32–37.

Stalder R., Ulmer P., Thompson A. B., and Gunther D. (2001) Experimental approach to constrain second critical end point in fluid/silicate systems: Near-solidus fluids and melts in the system albite-H_2O. *Am. Mineral.* **85,** 68–77.

Utsumi W., Funakoshi K., Urakawa S., Yamakata M., Tsuji K., Konishi H., and Shimomura O. (1998) SPring-8 beamlines for high pressure science with multi-anvil apparatus. *Rev. High Press. Sci. Technol.* **7,** 1484–1486.

Wyllie P. J. and Tuttle O. F. (1960) Experimental investigation of silicate systems containing two volatile components, Part 1. Geochemical considerations. *Am. J. Sci.* **258,** 498–517.

Yagi T., Shimomura O., Yamaoka S., Takemura K., and Akimoto S. (1985) Precise measurement of compressibility of gold at room and high temperatures. In *Solid State Physics under Pressure* (ed. S. Minomura), pp. 363–368. Terra Pub.

Yoder H. S. Jr., Stewart D. B., and Smith J. R. (1957) Ternary feldspars. *Year Book Carnegie Inst. Wash.* **56,** 206–214.